Switching Control in Vibration Isolation Systems

Marcel F. Heertjes, Ismail Hakki Sahin, Nathan van de Wouw, and W. P. Maurice H. Heemels

***Abstract*—In this paper, a switching control approach for active vibration isolation systems is proposed. The switching involves two regimes. In the first regime, no feedback control is applied thereby giving a low sensitivity to noise. In the second regime, active control induces improved disturbance rejection properties, but at the cost of increased noise sensitivity. Conditions for the stability of the switching closed-loop system are formulated whereas the stability analysis provides design rules for tuning the switching controller. Given this novel active vibration isolation approach, improved isolation performance is obtained with substantially less control authority in comparison to the case of linear (or non-switching) feedback control. Performance analysis is based on multi-resolution time-frequency analysis using measurements taken from a commercial vibration isolation system.**

***Index Terms*—Absolute stability, discontinuous variable gains, input-to-state stability, switching systems, vibration isolation, wavelet analysis.**

I. Introduction

IN HIGH-PRECISION motion systems, vibration isolation is used to isolate (sub-)systems from environmental disturbances such as floor vibrations and acoustic excitations. Examples include electron microscopes for nano-scale imaging and wafer scanners for the manufacturing of integrated circuits [5]. In these systems, vibration isolation performance is obtained both passively and actively. Typically, active vibration isolation involves both feedforward and feedback control [15], [19], [24]. In terms of feedback control, the discrimination between low-frequency disturbances for which the isolated system is sensitive and high-frequency disturbances for which it is not is crucial in achieving isolation performance [13], [14]. The additional discrimination between small-amplitude steady-state responses and large-amplitude transients provides the motivation to improve this performance even further, in particular, using a switching control approach [9], [20].

Envisioning such improvements starts with the observation that passive isolation typically relates to steady-state operation, i.e., the kind of isolation for which the isolator is designed to achieve performance. Only in the incident of having large-amplitude transient responses (and corresponding disturbances) active control is actually needed to improve upon the error response. In fact, the injection of additional (measurement) noise resulting from closing the loop is highly undesirable and can be avoided by adopting the following switching control strategy. Feedback control is switched on only when the error response exceeds a pre-defined threshold, thereby suppressing any further increase in transient response. Below this threshold, feedback control is switched off. This keeps the steady-state response limited in amplitude while the high-frequency isolation properties corresponding to the passive isolator design remain valid. In this way, the control authority is kept small and so is the injection of noise by closing the loop.

A comparable strategy is known to improve upon the disturbance rejection properties of optical storage drives [1], [11]. The approach in this paper is different because of the discontinuous nature of the switching. As it is known that favorable properties of the subsystems between which the closed-loop system switches (e.g., stability in the face of perturbations) are not always maintained, this strategy requires careful analysis and design of the resulting closed-loop system. For the vibration isolation problem, it will be shown that favorable stability properties of both the passive and the active isolation system remain in effect under the switching control approach; see [8] and [25] for different approaches but in the same context. Hereto the concept of input-to-state stability [21] is used along with extensions of absolute stability theory [23], [18]. The stability analysis provides design rules for the switching controller in view of isolation performance. The effectiveness of the approach in achieving improved servo performance is demonstrated using wavelet analysis [4], [7] applied to experimental data. Via a multi-resolution time-frequency approach the advantage of the switching becomes much clearer especially from the perspective of non-stationary servo performance.

This paper has the following five main contributions.

1) The design is presented of a switching feedback controller for vibration isolation systems with the aim to effectively combine favorable steady-state noise properties of the passive isolation system with improved disturbance rejection properties of transients under feedback control.
2) Conditions are formulated under which the switching closed-loop system is stable in the face of perturbations.
3) Design rules are presented for the switching controller ensuring that favorable passive noise sensitivity properties are preserved in steady-state.
4) The multi-resolution time-frequency analysis tool is employed as an effective means to illustrate improved isolation performance.
5) The main ideas such as developed in this paper are demonstrated using real experiments on a commercial vibration isolation system.

Manuscript received June 01, 2011; revised October 21, 2011; accepted January 24, 2012. Manuscript received in final form February 13, 2012. Date of publication March 21, 2012; date of current version nulldate. This work was supported by the Dutch Technology Foundation STW. Recommended by Associate Editor C. Bohn.

M. F. Heertjes is with the Department of Mechanical Engineering, Eindhoven University of Technology, 5600 MB Eindhoven, The Netherlands, and also with the Mechatronics System Development, ASML Netherlands B.V., 5504 DR Veldhoven, The Netherlands (e-mail: m.f.heertjes@tue.nl; marcel.heertjes@asml.com).

I. H. Sahin, N. van de Wouw, and W. P. M. H. Heemels are with the Department of Mechanical Engineering, Eindhoven University of Technology, 5600 MB Eindhoven, The Netherlands (e-mail: i.h.sahin@tue.nl; n.v.d.wouw@tue.nl; w.p.m.h.heemels@tue.nl).

Color versions of one or more of the figures in this paper are available online at http://ieeexplore.ieee.org.

Digital Object Identifier 10.1109/TCST.2012.2188294

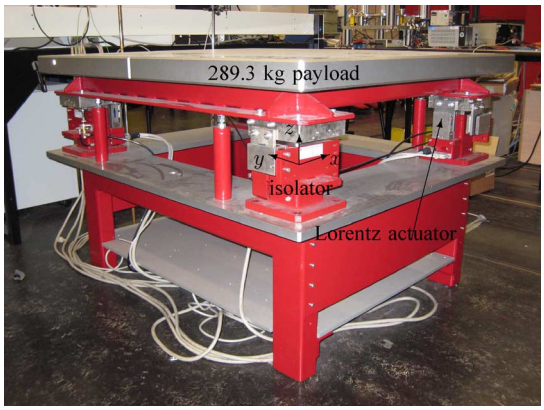

Fig. 1. Vibration isolation system from IDE.

In presenting the work, the following organization is adopted. In Section II, the vibration isolation system under study is discussed and the vibration isolation problem is formulated. In Section III, the switching control strategy is introduced as a means to improve upon isolator performance by active (sky-hook) damping. In Section IV, the stability properties of the switched closed-loop system in the face of perturbations are studied. Section V addresses the performance-based tuning of the switching controller whereas experimental results are presented in Section VI. Section VII contains the main conclusions. The wavelet analysis tool used throughout the paper is addressed in the Appendix.

Notation

$\mathbb{R}$ denotes real numbers and $\mathbb{R}_+$ denotes all non-negative real numbers. The maximum and minimum eigenvalues of a symmetric matrix $A \in \mathbb{R}^{n\times n}$ are denoted by $\lambda_{\max}(A)$ and $\lambda_{\min}(A)$ respectively. A symmetric matrix $A \in \mathbb{R}^{n\times n}$ is called positive definite if $x^T Ax > 0$ for all $x \in \mathbb{R}^n$, $x \neq 0$. This condition will be denoted by $A \succ 0$. For positive semi-definite matrix operators ($\succ$) is replaced by ($\succeq$). Furthermore $|.|$ denotes the Euclidian vector norm and $\|d_{[0,t]}\| = \sup_{\tau\in[0,t]}|d(\tau)|$ denotes the L_∞ norm of a signal $d : \mathbb{R}_+ \to \mathbb{R}^n$ on the interval $[0, t]$.

II. Vibration Isolation

Vibration isolation is used (for example) in the wafer scanner industry to isolate a metrology frame from environmental disturbances [12]. An example of a metrology frame is depicted in Fig. 1. It shows a payload mass of 289.3 kg, which is supported by pneumatic isolators. The natural frequency of the passive system in vertical direction is 3.24 Hz. The behavior of the isolation system is shown in Fig. 2. Through multi-resolution time-frequency analysis, the figure shows the scaled magnitude of the velocity response (z) of the payload in vertical direction both in the time- and frequency-domain; see the Appendix regarding the conducted wavelet analysis. The magnitude is linearly scaled from white (small) to black (large). In the weakly-damped response, large non-stationary oscillations near 3.24 Hz are recognized. At certain time intervals the system clearly oscillates at this frequency, at other time intervals it does not. In the high-frequency range the response merely shows small amplitude behavior. So the passive isolator design suggests favorable high-frequency isolation properties.

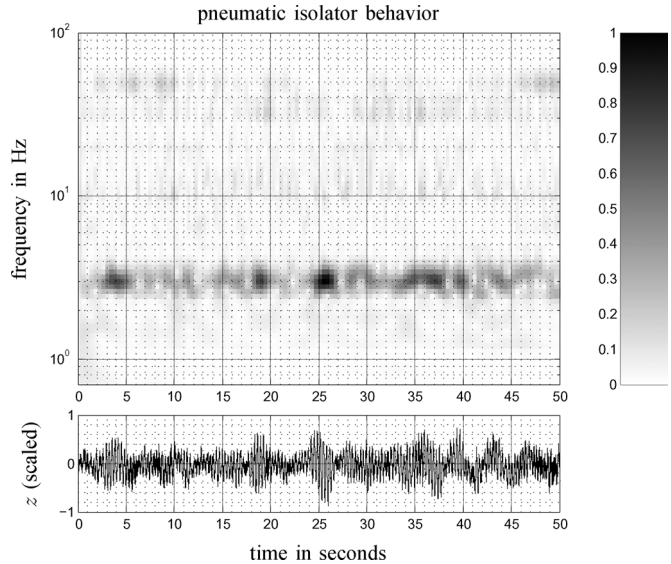

Fig. 2. Multi-resolution time-frequency analysis of the measured vertical velocities of the passive system.

The problem considered in this paper is the following. Design a switching controller to actively damp the low-frequency oscillations still present in the passive isolation system, see Fig. 2, while at the same time preserving the favorable high-frequency isolation properties of this passive (and undamped) system [14]. More specifically, the aim is to avoid deterioration of high-frequency transmissibility induced by passive damping [2], [26]. This deterioration generally follows from the transition of a -40 dB/dec sensitivity to floor disturbances for undamped mass-spring systems to a -20 dB/dec sensitivity in the case of passive damping.

III. Active Damping by Switching Control

To improve the payload response, i.e., to reduce the oscillations around the resonance frequency of the passive isolator, active (sky-hook) damping is applied [15]. Given linear motors of the Lorentz-type and geophones for velocity measurement [10] a simplified and single degree-of-freedom (DOF) schematic representation of the considered control configuration is shown in Fig. 3. Given a proper rigid-body decoupling, the single-axis case can easily be extended to a multi-axis case by considering for example the six individual rigid-body directions of motion [12]. In the figure, y is the payload displacement, $\dot{y}$ the corresponding velocity, f_c is the controller force, d_g represent ground vibrations, f_d is an external perturbation, and n is measurement noise on the velocity measurement $z = \dot{y} + n$. The plant represented by the transfer function $\mathcal{H}(s)$ between input (force) and output (displacement) is given by the following fourth-order model:

$$\mathcal{H}(s) = \frac{m_2 s^2 + b_{12} s + k_{12}}{m_1 m_2 s^4 + (m_1 + m_2)(b_{12} s^3 + k_{12} s^2)} \qquad (1)$$

with $m_1 = 274.8$ kg, $m_2 = 14.5$ kg, $b_{12} = 90$ Nsm^{-1}, $k_{12} = 5 \cdot 10^5$ Nm^{-1}, and $s \in \mathbb{C}$ denoting the Laplace variable. Let ϕ be a constant-valued gain with $\phi = 1$ in the case of linear

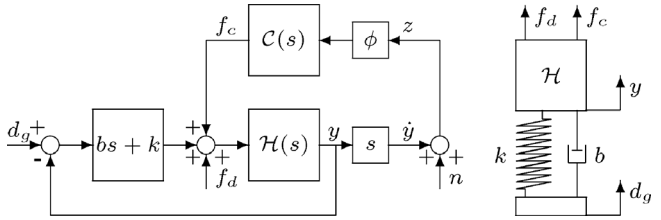

Fig. 3. Schematic of a controlled vibration isolator along with a mechanical representation.

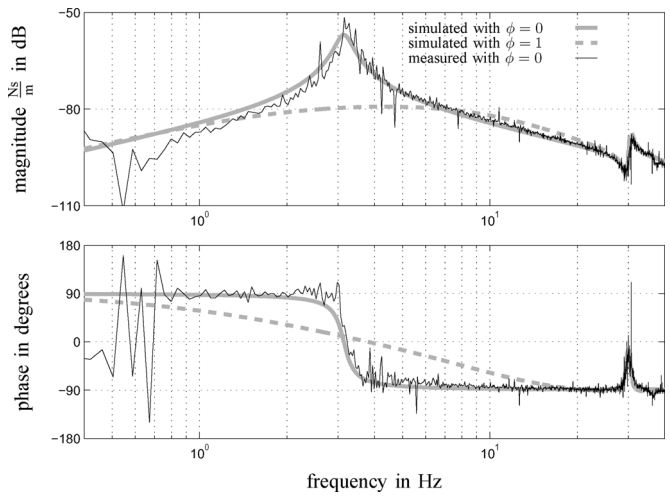

Fig. 4. Bode representation of the isolator characteristics $\mathcal{S}_p$ with ($\phi(z) = 1$) or without ($\phi(z) = 0$) control.

control. The controller transfer $\mathcal{C}(s)$ from $\dot{y}$ to f_c is then chosen as

$$\mathcal{C}(s) = k_d \left\{ \frac{s}{s+\omega_{hp}} \right\}^2 \left\{ \frac{\omega_{lp}}{s+\omega_{lp}} \right\}^2 \tag{2}$$

with $k_d = 3 \cdot 10^4$ Nsm^{-1} a gain, ω_{hp} the crossover frequency of a second-order high-pass filter, and ω_{lp} the roll-off frequency of a second-order low-pass filter. $\mathcal{C}(s)$ reflects a complex-valued damper and is used to improve disturbance rejection near resonance without significantly deteriorating the passive isolation properties; the latter being characterized by the isolator stiffness $k = 1.1 \cdot 10^5$ Nm^{-1} and the damping coefficient $b = 7 \cdot 10^2$ Nsm^{-1} in combination with $\mathcal{H}(s)$. Sensor limitations typically occur below 0.1 Hz and lead to the choice for $\omega_{hp} = 0.2\pi$ rad/s. Actuator limitations occur beyond 100 Hz, which lead to the choice for $\omega_{lp} = 200\pi$ rad/s.

The closed-loop characteristics given by the transfer from f_d to $\dot{y}$, or

$$\mathcal{S}_p(s) = \frac{s\mathcal{H}(s)}{1 + (bs+k)\mathcal{H}(s) + s\phi\mathcal{C}(s)\mathcal{H}(s)} \tag{3}$$

are depicted in Fig. 4 (for $s = 2\pi j f$ and frequency f) either with ($\phi = 1$) or without ($\phi = 0$) control. The Bode plots show both numerical and experimental results. From the figure, it is clear that isolator performance benefits from the given linear control strategy. The sensitivity near the natural frequency is much improved at the cost of seemingly small low- and high-frequency deterioration.

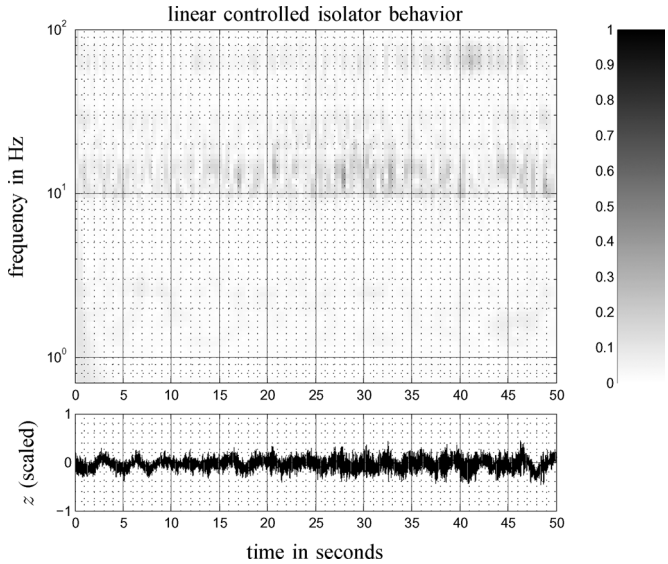

Fig. 5. Time-frequency analysis of the measured and linear controlled velocities (scales adopted from Fig. 2).

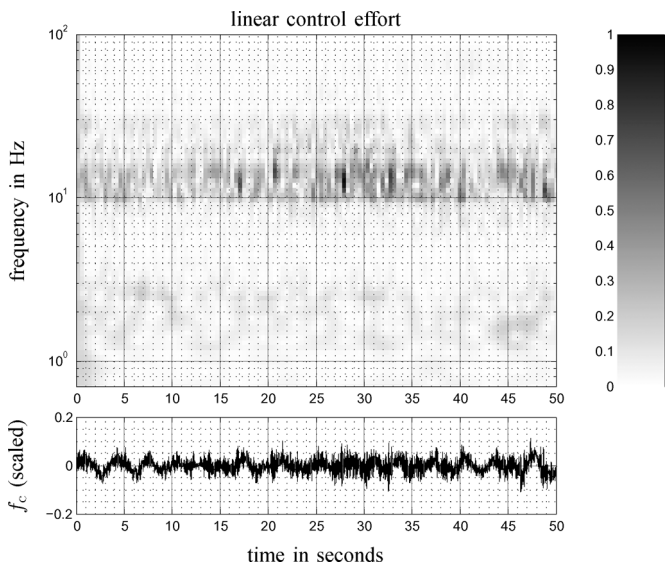

Fig. 6. Time-frequency analysis of the measured control forces.

The validity of this observation is disclosed in more detail in Fig. 5 using multi-resolution time-frequency analysis. In comparison with Fig. 2, it can be seen that the velocity response is indeed significantly reduced in amplitude. In fact, the non-stationary oscillations dominated by the natural frequency of the passive isolator around 3.24 Hz seem no longer present. However, high-frequency noise (between 10–20 Hz) tends to be amplified. This directly follows from Bode's sensitivity integral in which the peak of the sensitivity function is shifted from 3.24 Hz without ($\phi = 0$) control to 10.8 Hz with ($\phi = 1$) control. This is seen more clearly in Fig. 6 by subjecting the corresponding scaled control force f_c to a similar analysis. It can be seen that the linear controller induces a significant high-frequency control signal. This is undesirable as it potentially compromises high-frequency passive vibration isolation.

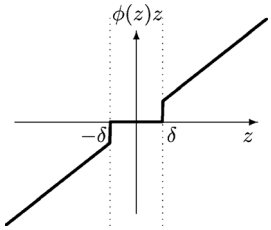

Fig. 7. Switching characteristic of $z \mapsto \phi(z)z$.

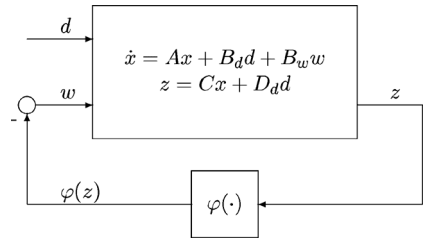

Fig. 8. Closed-loop plant with sector nonlinearity.

These observations hint toward the application of switching control. Sporadically switching the control on improves the resonance-induced isolator response related to large-amplitude transients. Switching the control off restores the passive isolation properties, which are favorable in view of low-amplitude (and high-frequency) measurement noise. The idea can be formalized by selecting the switching gain function ϕ in Fig. 3 as

$$\phi(z) := \begin{cases} 0, & \text{if } |z| \leq \delta \\ 1, & \text{otherwise} \end{cases} \tag{4}$$

with $\delta \geq 0$ a threshold parameter. This switching gain function discriminates between control ($\phi(z)z = z$) and no control ($\phi(z)z = 0$) on the basis of the magnitude of the input signal $z = \dot{y} + n$. The characteristics of $z \mapsto \phi(z)z$ are depicted in Fig. 7. With such a discontinuous element in the loop, analysis of the switching closed-loop system becomes nontrivial and requires a thorough study of its stability and performance properties to substantiate the intuitive benefit of the switching strategy [6], [17].

IV. Stability of the Switching Closed-Loop System

To study stability of the switching closed-loop system in the face of perturbations, it is important to distinguish between transient and steady-state disturbances. Transient disturbances, related to the external disturbances f_d and d_g are assumed to occur incidentally. When present, they often cause the system to react heavily in terms of error response. Control then mainly improves upon this response. Contrarily, steady-state disturbances caused by measurement noise n are typically of small amplitude. In this case, it is preferred to switch the controller off in order to eliminate the sensitivity to measurement noise entirely. For the switching controller this is guaranteed if the steady-state response under measurement noise satisfies $|z| = |\dot{y} + n| \leq \delta$. Consequently, this requires that the given threshold value δ should be designed such that it encapsulates the steady-state response induced by the persistent measurement noise n. In turn, this restores the favorable passive isolation properties in the absence of transient disturbances. From a stability point of view, it is therefore sufficient to require that control, if applied, forces the system response toward the uncontrolled (passive) steady-state. To show this the concept of input-to-state stability (ISS) [21] will be used. In particular it is shown, first, that the closed-loop system will exhibit bounded responses to *any* bounded disturbance including both transient and steady-state disturbances and, second, ISS will be used to select the threshold value δ such that passive isolation behavior will be retained in the absence of these transient disturbances.

Input-to-state stability is studied using the following state-space system representation of the closed-loop system:

$$\begin{aligned} \dot{x} &= Ax + B_d d + B_w w \\ z &= Cx + D_d d \\ w &= -\varphi(z) \end{aligned} \tag{5}$$

see also Fig. 8.

The state vector x is defined by

$$x := [\, x_p^T \quad x_c^T \,]^T \in \mathbb{R}^8 \tag{6}$$

with the state variables x_p and x_c, respectively, related to a state-space realization of the plant and controller given in (1) and (2). The bounded disturbance vector d is defined by combining all disturbance sources in Fig. 3, including the ground velocity $\dot{d}_g$

$$d := [\, f_d \quad d_g \quad \dot{d}_g \quad n \,]^T \in \mathbb{R}^4. \tag{7}$$

The memoryless nonlinearity $\varphi(z)$ in (5) is related to the switching gain function $\phi(z)$ in (4) by

$$\varphi(z) := \phi(z)z, \;\; z \in \mathbb{R}. \tag{8}$$

In (5), the constant matrices $A \in \mathbb{R}^{8\times 8}$, $B_d \in \mathbb{R}^{8\times 4}$, $B_w \in \mathbb{R}^{8\times 1}$, $C \in \mathbb{R}^{1\times 8}$, and $D_d \in \mathbb{R}^{1\times 4}$ are given by

$$\begin{aligned} A &:= \begin{bmatrix} \tilde{A}_p & \tilde{B}_{p,u}\tilde{C}_c \\ 0 & \tilde{A}_c \end{bmatrix}, B_d := \begin{bmatrix} \tilde{B}_{p,d} \\ 0 \end{bmatrix} \\ B_w &:= \begin{bmatrix} \tilde{B}_{p,u}\tilde{D}_c \\ \tilde{B}_c \end{bmatrix}, C := [\, \tilde{C}_p \quad 0 \,], D_d := [\, \tilde{D}_{p,d} \,] \end{aligned} \tag{9}$$

with the plant-related matrices $\tilde{A}_p \in \mathbb{R}^{4\times 4}$, $\tilde{B}_{p,d} \in \mathbb{R}^{4\times 4}$

$$\tilde{A}_p = \begin{bmatrix} 0 & 1 & 0 & 0 \\ \frac{-k_{12}}{m_2} & \frac{-b_{12}}{m_2} & \frac{k_{12}}{m_2} & \frac{b_{12}}{m_2} \\ 0 & 0 & 0 & 1 \\ \frac{k_{12}}{m_1} & \frac{b_{12}}{m_1} & \frac{-(k+k_{12})}{m_1} & \frac{-(b+b_{12})}{m_1} \end{bmatrix}$$

$$\tilde{B}_{p,d} = \begin{bmatrix} 0 & 0 & 0 & 0 \\ 0 & 0 & 0 & 0 \\ 0 & 0 & 0 & 0 \\ \frac{1}{m_1} & \frac{k}{m_1} & \frac{b}{m_1} & 0 \end{bmatrix}, \tilde{B}_{p,u} = \begin{bmatrix} 0 \\ 0 \\ 0 \\ \frac{1}{m_1} \end{bmatrix}$$

$$\tilde{C}_p = [\, 0 \quad 0 \quad 0 \quad -1 \,], \tilde{D}_{p,d} = [\, 0 \quad 0 \quad 0 \quad -1 \,]$$

and the controller-related matrices $\tilde{A}_c \in \mathbb{R}^{4\times 4}$, $\tilde{B}_c \in \mathbb{R}^{4\times 1}$, $\tilde{C}_c \in \mathbb{R}^{1\times 4}$, and $\tilde{D}_c \in \mathbb{R}$ given by

$$\tilde{A}_c^T = \begin{bmatrix} 0 & 0 & 0 & -\omega_{lp}^2\omega_{hp}^2 \\ 1 & 0 & 0 & -2\omega_{lp}\omega_{hp}(\omega_{hp} + \omega_{lp}) \\ 0 & 1 & 0 & -(\omega_{lp}^2 + \omega_{hp}^2 + 4\omega_{hp}\omega_{lp}) \\ 0 & 0 & 1 & -2(\omega_{lp} + \omega_{hp}) \end{bmatrix}$$

$$\tilde{B}_c = \begin{bmatrix} 0 \\ 0 \\ 0 \\ -k_d\omega_{lp}^2 \end{bmatrix}, \tilde{C}_c^T = \begin{bmatrix} 0 \\ 0 \\ -1 \\ 0 \end{bmatrix}, \tilde{D}_c = [\,0\,]$$

which corresponds to the state-space realization of (1) and (2), combined with the control configuration given in Fig. 3.

System (5) is said to be input-to-state stable [21], if

$$|x(t)| \leq \beta(|x_0|, t) + \gamma(\|d_{[0,t]}\|) \tag{10}$$

holds for all solutions of (5) where β is a so-called $\mathcal{KL}$-function and γ a $\mathcal{K}$-function (see [21] for the details). As such, functions are sought of the form $\beta(s,t) = ce^{-at}s$ and $\gamma(s) = \gamma s, s \in \mathbb{R}_+$, $t \in \mathbb{R}_+$, for $c \geq 0$, $a > 0$, and $\gamma \geq 0$. Since the effect of initial conditions through β eventually fades away, γ refers to the ISS gain.

To prove ISS for system (5), let $V(x) = x^T P x$ be an ISS Lyapunov function candidate with $x \in \mathbb{R}^n$, for a positive definite matrix $P = P^T \succ 0$. Note that

$$c_1|x|^2 \leq V(x) \leq c_2|x|^2 \text{ for all } x \in \mathbb{R}^8 \tag{11}$$

where c_1 and c_2 are defined as

$$c_1 := \lambda_{\min}(P) \qquad c_2 := \lambda_{\max}(P). \tag{12}$$

If there exist $\alpha > 0$ and $\sigma > 0$ such that along solutions of (5), it holds for all $t \in \mathbb{R}_+$ that

$$\dot{V}(x) \leq -\alpha x^T x + \sigma d^T d \tag{13}$$

then $V(x)$ is an ISS Lyapunov function for (5). The requirement on the time-derivative of $V(x)$ in (13) can be written as

$$\begin{aligned}\dot{V}(x) = x^T(A^TP + PA)x + d^T B_d^T P x + w^T B_w^T P x \\ + x^T P B_d d + x^T P B_w w \leq -\alpha x^T x + \sigma d^T d\end{aligned} \tag{14}$$

or, alternatively

$$\begin{aligned}\begin{pmatrix} x \\ d \\ w \end{pmatrix}^T \begin{pmatrix} PA + A^TP & PB_d & PB_w \\ B_d^TP & 0 & 0 \\ B_w^TP & 0 & 0 \end{pmatrix} \begin{pmatrix} x \\ d \\ w \end{pmatrix} \\ \leq -\alpha x^T x + \sigma d^T d\end{aligned} \tag{15}$$

which should hold for all $x \in \mathbb{R}^8$, $d \in \mathbb{R}^4$, and $w \in \mathbb{R}$. Since w is the output to the sector-bounded nonlinearity $\varphi(z)$ [see (5)] inequality (15) is only required to hold for x, d, and w satisfying $w^T z \leq -w^T w$, which corresponds to the $[0, 1]$ sector for $\varphi(z)$. By using the expression for z in (5), the sector condition can be rewritten as

$$\begin{pmatrix} x \\ d \\ w \end{pmatrix}^T \begin{pmatrix} 0 & 0 & \frac{1}{2}C^T \\ 0 & 0 & \frac{1}{2}D_d^T \\ \frac{1}{2}C & \frac{1}{2}D_d & 1 \end{pmatrix} \begin{pmatrix} x \\ d \\ w \end{pmatrix} \leq 0 \tag{16}$$

for $x \in \mathbb{R}^8$, $d \in \mathbb{R}^4$, and $w \in \mathbb{R}$. To prove ISS of (5), inequality (15) needs to be satisfied while (16) holds. By applying the S-procedure [3], this results in the following linear matrix inequalities (LMIs):

$$\begin{pmatrix} PA + A^TP + \alpha I & PB_d & PB_w - \frac{1}{2}\tau C^T \\ B_d^TP & -\sigma I & -\frac{1}{2}\tau D_d^T \\ B_w^TP - \frac{1}{2}\tau C & -\frac{1}{2}\tau D_d & -\tau \end{pmatrix} \preceq 0. \tag{17}$$

Hence, if $P = P^T \succ 0$, $\alpha > 0$, $\sigma > 0$, and $\tau > 0$ are found such that (17) holds, then ISS of (5) is proved.

Remark 1: Interestingly, the existence of $P = P^T \succ 0$ in (17) *implies that the LMI*

$$\begin{pmatrix} A^TP + PA + \epsilon P & PB_w - \frac{1}{2}\tau C^T \\ B_w^TP - \frac{1}{2}\tau C & -\tau \end{pmatrix} \preceq 0 \tag{18}$$

is feasible for sufficiently small $\epsilon > 0$, which is equivalent to the following frequency domain condition

$$\begin{pmatrix} G_w(j\omega) \\ 1 \end{pmatrix}^T \begin{pmatrix} 0 & -\frac{1}{2}\tau \\ -\frac{1}{2}\tau & -\tau \end{pmatrix} \begin{pmatrix} G_w(j\omega) \\ 1 \end{pmatrix} \preceq 0, \quad \omega \in \mathbb{R} \tag{19}$$

resulting from the Kalman-Yakubovich-Popov lemma [16], where $G_w(j\omega) := C(j\omega I - A)^{-1}B_w$. Simplifying (19) *gives*

$$\mathfrak{R}e\{C(j\omega I - A)^{-1}B_w\} \geq -1, \quad \omega \in \mathbb{R} \tag{20}$$

which is the circle criterion condition for the $[0, 1]$ sector [23]. Feasibility of the circle criterion LMI in (18) *implies feasibility of the LMI in* (17) *for a sufficiently large value of $\sigma > 0$. By solving* (18)*, it can therefore be shown that the system is ISS for some $\sigma > 0$, which enables the computation of an upper bound on the ISS gain. But the smallest ISS gain based on a solution of* (18) *is usually conservative, since it relates to the particular choice of P satisfying* (18)*. Therefore, it is proposed to solve* (17) *instead and minimize the variable σ, which then indirectly leads to minimization of the ISS gain.*

If there exists an ISS Lyapunov function $V(x) = x^T P x$, $x \in \mathbb{R}^n$, satisfying (17) and $P = P^T \succ 0$, then the solution trajectory is bounded according to

$$|x(t)| \leq \beta(|x_0|, t) + \gamma\|d_{[0,t]}\| \tag{21}$$

where β and γ are defined as

$$\beta(|x_0|, t) := \sqrt{\frac{c_2}{c_1}} e^{-(\epsilon t/2c_2)}|x_0| \tag{22}$$

$$\gamma := \sqrt{\frac{c_2}{c_1}\frac{\sigma}{\alpha - \epsilon}}. \tag{23}$$

Under condition (17) and $P = P^T \succ 0$ it is therefore concluded that (5) is ISS with respect to the disturbance vector d. Observe that σ (and c_1, c_2, α) influences the ISS gain γ. Furthermore, note that the stability analysis refers to the single-axis isolator model in Fig. 3. The possible extension to multi-axis isolators, for example, by including horizontal and/or rotational axes next to the considered vertical axis, mainly depends on the ability to decouple the resulting MIMO plant dynamics. For a decoupled plant, a diagonal controller structure allows for extension of the

results. For a coupled plant, such an extension is generally nontrivial.

V. Performance-Based Design of the Switching Controller

Returning to the vibration isolation control problem, recall that the bounded disturbances f_d, d_g, and $\dot{d}_g$ typically have a transient nature. Contrarily, the persistent measurement noise n relates to the steady-state behavior of the closed-loop system. Since control is used to improve upon the transient response, the threshold parameter δ should be designed such that in steady-state, control is switched off and passive isolation is retained. So δ should be designed as small as possible to attain the best suppression of transient disturbances without substantially compromising measurement noise sensitivity. For this purpose, the smallest ISS gain γ as in (23) is sought.

Minimizing the ISS gain γ is done through fixing α and minimizing σ while putting a lower bound on c_1. Using (21), the minimum ultimate bound on the state x with respect to measurement noise n becomes

$$\limsup_{t\to\infty} |x(t)| \leq \gamma \|n_{[0,\infty]}\|. \tag{24}$$

Since the goal is to find the minimum ultimate bound on the output $z = \dot{y} + n$, the ultimate bound on z can be directly computed as

$$\limsup_{t\to\infty} |z(t)| \leq \gamma_{n\to z} \|n_{[0,\infty]}\| \tag{25}$$

where

$$\gamma_{n\to z} = \gamma |C| + 1. \tag{26}$$

In finding $\gamma_{n\to z}$, the matrix $P = P^T \succ 0$ is computed by solving the LMIs given in (17). A small positive number for $\epsilon = 10^{-6}$ is selected, since the goal is not to obtain large exponential decay rates, $\alpha = 1$ is fixed, and $\sigma > 0$ and $\tau > 0$ are left as free variables. Recall from the discussion near the end of the previous section that the ISS gain γ is found indirectly by solving (17) and minimize the variable σ. This gives $\sigma = 0.3121$, $\tau = 1.0673$, and P as in (27). See equation (27) at the bottom of the page. Furthermore, with (12) it follows that $c_1 = 0.0101$ and $c_2 = 5.6744$ which combined with the values for σ, α, and ϵ according to (23) yield the ISS gain as $\gamma = 13.2430$. Using a balanced realization of (5) with C and C^T-matrix

$$C^T = \begin{bmatrix} -4.423 \\ -0.010 \\ 0.414 \\ -0.141 \\ 4.819 \\ -0.011 \\ 1.873 \\ 0.002 \end{bmatrix} \tag{28}$$

an ultimate bound on the output z follows from (25) with

$$\gamma_{n\to z} = 91.29. \tag{29}$$

But this bound is conservative since it employs $|C| = \sqrt{\lambda_{\max}(C^T C)}$, see (26). Therefore, instead of using an ultimate bound on x, the existence is utilized of a positively invariant set to which all solutions converge. More specifically, from ISS analysis it can be shown that Ω_μ defined in

$$\Omega_\mu = \{x \in \mathbb{R}^n | x^T P x \leq \mu\} \tag{30}$$

is a positively invariant set where $\mu > 0$ is defined as

$$\mu = c_2 \frac{\sigma}{\alpha - \epsilon} \|n_{[0,\infty]}\|. \tag{31}$$

Using the level set of $V(x) = x^T P x$, it therefore is possible to find the maximum value that $|\dot{y}|^2$ can take inside the set Ω_μ. In so doing, $\max |\dot{y}|$ subject to $x^T P x = \mu$ needs to be computed where (due to symmetry) $\max \dot{y} = \max |\dot{y}|$.

The Lagrange multiplier method is employed in order to solve such a maximization problem. First, the objective function and constraints are defined as follows:

$$\max \quad Cx \tag{32}$$

$$\text{subject to } x^T P x = \mu. \tag{33}$$

Second, the Lagrangian function is defined as

$$L(x, \lambda) := Cx + \lambda(x^T P x - \mu) \tag{34}$$

$$P = \begin{bmatrix} 0.5430 & 0.0280 & -0.0002 & 0.0056 & 0.0109 & -0.0141 & -0.0017 & 0.0032 \\ 0.0280 & 0.5428 & 0.0022 & -0.0003 & 0.0080 & -0.0141 & -0.0015 & -0.0019 \\ -0.0002 & 0.0022 & 0.6946 & -0.0100 & -0.0759 & 0.0026 & 0.0102 & 0.0011 \\ 0.0056 & -0.0003 & -0.0100 & 0.6872 & -0.0328 & -0.0214 & 0.0130 & 0.0050 \\ 0.0109 & 0.0080 & -0.0759 & -0.0328 & 0.1088 & -0.0681 & -0.0070 & 0.0412 \\ -0.0141 & -0.0141 & 0.0026 & -0.0214 & -0.0681 & 1.3336 & 0.0354 & 0.7582 \\ -0.0017 & -0.0015 & 0.0102 & 0.0130 & -0.0070 & 0.0354 & 0.0132 & 0.1068 \\ 0.0032 & -0.0019 & 0.0011 & 0.0050 & 0.0412 & 0.7582 & 0.1068 & 5.5396 \end{bmatrix} \tag{27}$$

where λ is the Lagrange multiplier. By taking the partial derivatives of $L(x,\lambda)$ with respect to both x and λ the following stationary points are obtained:

$$\frac{\partial}{\partial x}L(x,\lambda) = C^T + \lambda(2Px) = 0 \tag{35}$$

$$\frac{\partial}{\partial \lambda}L(x,\lambda) = x^T Px - \mu = 0. \tag{36}$$

From (35) it follows for the state evaluated at these points that

$$x = -\frac{1}{2\lambda}P^{-1}C^T. \tag{37}$$

Now λ is computed by substituting (37) in (36) giving

$$\lambda = \frac{1}{2}\sqrt{\frac{CP^{-1}C^T}{\mu}}. \tag{38}$$

Combining the result (38) with (37) gives that

$$\max_{x\in\Omega_\mu}|Cx| = \sqrt{CP^{-1}C^T\mu}. \tag{39}$$

Given $z = \dot{y} + n$ and $\dot{y} = Cx$ the smallest ultimate bound on the measured output z with respect to n is found as

$$\limsup_{t\to\infty}|z(t)| \leq \gamma_{n\to z}\|n_{[0,\infty]}\| \tag{40}$$

where

$$\gamma_{n\to z} := 1 + \sqrt{CP^{-1}C^T c_2\frac{\sigma}{\alpha-\epsilon}}. \tag{41}$$

For (41) with P in (27), C and C^T in (28), $c_2 = 5.6744$, $\sigma = 0.3121$, $\alpha = 1$, and $\epsilon = 10^{-6}$, it follows that

$$\gamma_{n\to z} = 37.05. \tag{42}$$

In comparison with (29), (42) gives a less conservative (hence more realistic) bound. Using this bound in the controller design implies that the threshold parameter δ should be 37.05 times larger than the maximum amplitude of the measurement noise n in order to ensure that passive isolation properties are retained in the absence of transient disturbances.

A reasonable estimate for the maximum amplitude of the measurement noise n is directly related to the sensor properties. For the experimental setup under study, assume that the maximum measurement noise n is less than 0.5% of the maximum magnitude of the measured velocity signals. Then δ can be selected as 20% of the maximum magnitude of the measured signals which, given the gain band as in (42), guarantees that the steady-state response to measurement noise is within the threshold value and passive isolation in steady-state is preserved.

VI. Experimental Performance Analysis

In this section, performance of the switching control strategy is studied using experimental analysis. This includes a comparison to linear control and passive isolation.

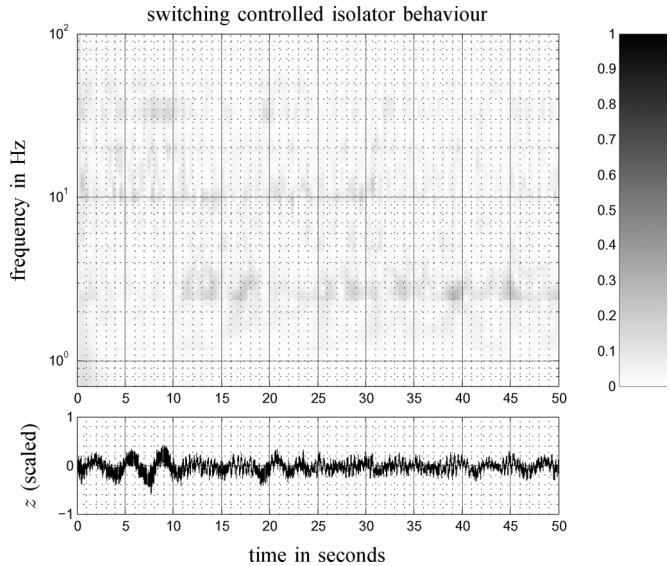

Fig. 9. Multi-resolution time-frequency analysis of the measured and switching controlled velocities (scales adopted from Figs. 2 and 5).

The experimental analysis is conducted using the setup in Fig. 1 from integrated dynamics engineering (IDE). Signal communication goes via a Quansar Q8 measurement and control board with six analog inputs and eight analogue outputs. This board has 14-bit analog-to-digital (A/D) converters, 12-bit digital-to-analog (D/A) converters, and samples its communication channels up to 100 kHz. The inputs contain the sensor information of six geophones amplified by voltage amplifiers. The outputs represent the control signals which are fed to current amplifiers. Through eight linear motors, this provides the control forces to the isolation system. Both actuators and sensors are over-dimensioned such that actuator and sensor saturation is strictly avoided. In the high-precision motion industry this is seen often; see [22] for an approach in dealing with saturation in the control design. The measurement and control board is connected to a host computer via an RS-232 communications link. The host computer is used to generate the control signals via xPC Target in combination with a C-compiler and the control design in MATLAB/Simulink.

The result of the switching control in terms of measured isolator response is shown in Fig. 9. The choice for $\delta = 0.2$ relates to the numerical calculations given at the end of the previous section whereas the peak value of the measured velocity signals is scaled to one; switching occurs at 20% of this peak value. Similar to the linearly controlled isolator characteristics of Fig. 5, the non-stationary oscillations related to the system's natural frequency at 3.24 Hz have almost disappeared. However the amplification of high-frequency noises is no longer present, that is, the high-frequency passive isolation properties are preserved. This is more clear when applying the multi-resolution time-frequency analysis to the switching (and scaled) control forces, which is shown in Fig. 10. As compared to the linear control forces depicted in Fig. 6, it can be seen that control is only applied in those time intervals where the error response exceeds the threshold parameter δ. For the remaining intervals, the control is switched off.

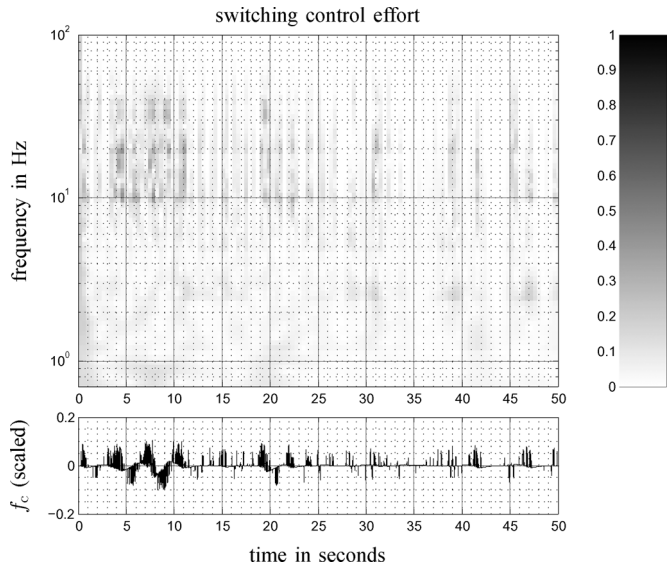

Fig. 10. Multi-resolution time-frequency analysis of the measured switching control forces (scales adopted from Fig. 6).

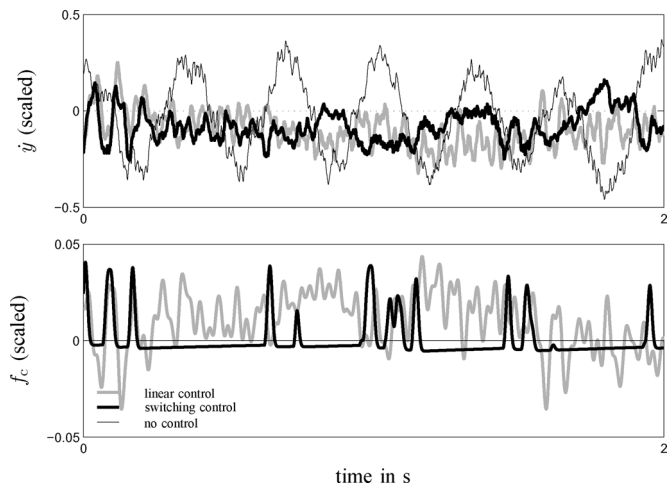

Fig. 11. Time-series measurement of the vertical velocities and control forces in the case of no control, linear control, and switching control.

In the time-domain signals, Fig. 11 more clearly illustrates the differences between the considered control strategies. For the scaled payload velocity in the vertical direction, it can be seen that no control yields the expression of large oscillations (thin black curves) dictated by the weakly damped resonance at 3.24 Hz. Under linear control these oscillations disappear (grey curves) but the velocity response shows increased high-frequency oscillatory behavior. Switching control provides an effective means in dealing with the system's resonance (thick black curves) but also limits the presence of high-frequency noise. This is due to the fact that control is only sporadically switched on (see the lower part of the figure) which has a beneficial effect on the control authority needed when compared to the linear controller.

Similar observations are obtained from the cumulative power spectral density (CPSD) analysis as can be found in Fig. 12. From this figure, it can be concluded that both linear and switching control yield comparable root-mean-square

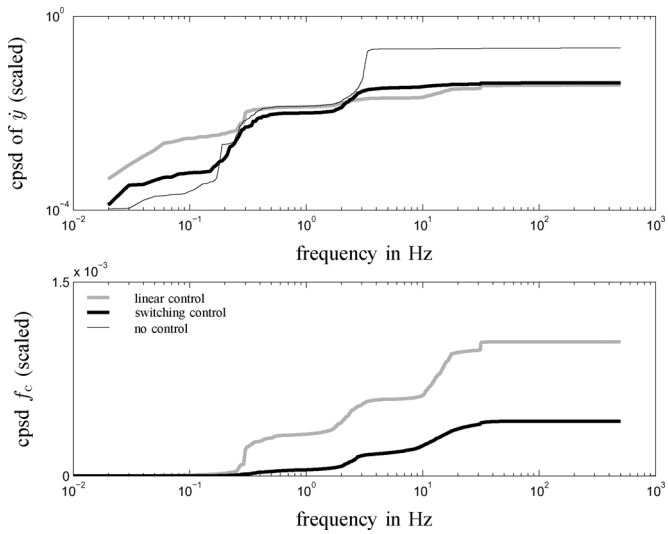

Fig. 12. CPSD analysis of the measured vertical velocities and control forces in the case of no control, linear control, and switching control.

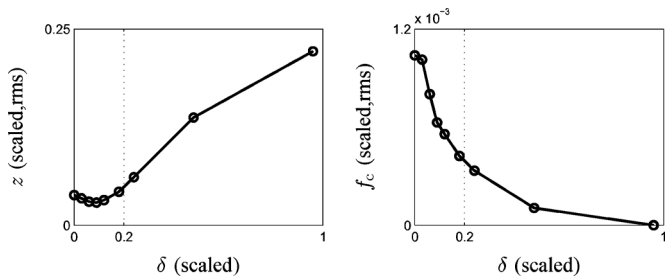

Fig. 13. rms values of the measured vertical velocities and control forces under variation of δ.

(rms) values of the scaled velocity signals. Each experiment corresponds to a time interval of 100 s in which a sampling frequency of 1 kHz is used. For switching control, the result is obtained with significantly less control effort, see bottom part in Fig. 12, thus giving limited transmission (and amplification) of noise through control.

The relation between rms-performance and control effort is addressed in Fig. 13. By considering several values for the threshold parameter δ and depicting the resulting rms-values of each corresponding experiment as a function of δ, it can be seen that for small enough δ the switching control competes with the linear control ($\delta = 0$) in terms of small rms-values. It comes, however, with less control effort. Also, this experimental performance analysis confirms that $\delta = 0.2$ is a reasonable design choice for guaranteeing a low velocity response under limited control authority.

VII. Conclusion

A switching control design is proposed and demonstrated to be effective in achieving improved active vibration isolation. A multi-resolution time-frequency analysis aids much to the interpretation of the results and the motivation for the switching. Sporadically switching the control on effectively removes transient oscillations from the velocity response. The amplification of steady-state noise by closing the loop is largely avoided by switching the control off at small velocities. Consequently, the

control effort is kept small while preserving the desired passive isolation properties. Stability of the switching closed-loop system in the face of perturbations is studied using the concept of input-to-state stability. The stability analysis also provides design rules for the switching controller aiming at performance. The benefit of the proposed control strategy is further evidenced by an experimental study on a commercial vibration isolation system.

APPENDIX

The multi-resolution time-frequency analysis used in this paper is centered about the Morlet wavelet ψ [4]

$$\psi(t) = e^{-\beta(t^2/2)} e^{j\omega_0 t} \tag{43}$$

where $\beta = 120$ and $\omega_o = 2\pi 15$ rad $\cdot$ s^{-1}. Because of the fast decay of the first exponential function in (43), the outer parts of the wavelet ($t \in [-\infty, 2)$ and $t \in (2, \infty]$) are neglected. The inner part is discretized with $\Delta t = 0.01$. The time-sampled input signal u (10^5 data points with 1 ms sampling time) is sequentially low-pass filtered and down-sampled [7]. Each down-sampling reduces the time-resolution but increases the frequency resolution. In decomposing u, the wavelet transformation matrix $\Gamma(u, \psi)$ is obtained by convolving the proper u and ψ along the number of filter banks $N_b = 8$ with a frequency resolution parameter per filter bank of $N_f = 10$ and a time resolution parameter of $N_t = 250$. The following script is used.

```
function
[time,frequencies,GammaMat] = dwt(u,Ts,beta,wo,Nt,Nf,Nb,dt)
%-------------------------------------------------------------
% dwt  = discrete wavelet transform
%-------------------------------------------------------------
% u    = data vector
% Ts   = data sampling time
% beta = first Morlet wavelet parameter
% wo   = second Morlet wavelet parameter
% Nt   = time resolution
% Nf   = frequency resolution per filter bank
% Nb   = number of filter banks
% dt   = wavelet time-discretization
time = linspace(0,(size(u,1)-1)*Ts,Nt);
frequencies =(wo/(2*pi))*dt/Ts*2.^-(0:1/Nf:(Nb-1/Nf));
%-------------------------------------------------------------
% 1. Morlet wavelet with compact support
%-------------------------------------------------------------
Tn = 2.^fliplr(0:1/Nf:(1-1/Nf));
for i = 1:Nf
 wt = -Tn(i):dt:Tn(i);
 psi = exp(j*wo*wt/Tn(i)).*exp(-beta*((wt/Tn(i)).^2)/2);
 wstruct.(['wstruct' num2str(i)]) = psi;
end
%-------------------------------------------------------------
% 2. decomposition filter banks
%-------------------------------------------------------------
[num,den] = butter(4,.5); y{1} = u;
for count = 1:Nb-1
 y{count+1} = downsample(filtfilt(num,den,y{count}),2);
end
%-------------------------------------------------------------
% 3. wavelet transform
%-------------------------------------------------------------
for i = 1:Nb
 for j = 1:Nf
  tf1 = conv(y{i},wstruct.(['wstruct' num2str(j)]));
  tf2 = el(tf1,size(y{i},1));
  GammaMat(Nf*(i-1)+(Nf+1-j),:) = rs(tf2',Nt);
 end
end
%-------------------------------------------------------------
% a. function rs (re_sample)
%-------------------------------------------------------------
function y = rs(x,Nt)
y = x(round(linspace(1,size(x,1),Nt)));
%-------------------------------------------------------------
% b. function el (equal length)
%-------------------------------------------------------------
function y = el(x,length_u) dl = size(x,1) - length_u;
y = x(floor(dl/2):floor(dl/2)+length_u-1);
```

REFERENCES

[1] B. S. R. Armstrong, J. A. Gutierrez, B. A. Wade, and R. Joseph, "Stability of phase-based gain modulation with designer-chosen switch functions," *Int. J. Robot. Res.*, vol. 25, pp. 781–796, 2006.

[2] S. Behrens, A. J. Fleming, and S. O. R. Moheimani, "Passive vibration control via electromagnetic shunt damping," *Trans. Mechatronics*, vol. 10, no. 1, pp. 118–122, 2005.

[3] S. P. Boyd, L. El Ghaoui, E. Feron, and V. Balakrishnan, "**<PLEASE PROVIDE VOLUME AND PAGE NUMBERS.>** Linear matrix inequalities in system and control theory," *Studies Appl. Math.*, 1994.

[4] R. Büssow, "An algorithm for the continuous Morlet wavelet transform," *Mechan. Syst. Signal Process.*, vol. 21, pp. 2970–2979, 2007.

[5] H. Butler, "Position control in lithographic equipment; An enabler for current-day chip manufacturing," *Control Syst. Mag.*, vol. 11, pp. 28–47, 2011.

[6] G. C. Cheng, K. Peng, B. M. Chen, and T. H. Lee, "Improving transient performance in tracking general references using composite nonlinear feedback control and its application to high-speed XY-table positioning mechanism," *Trans. Ind. Electron.*, vol. 54, no. 2, pp. 1039–1051, 2007.

[7] I. S. Cade, P. S. Keogh, and M. N. Sahinkaya, "Fault identification in rotor/magnetic bearing systems using discrete time wavelet coefficients," *Trans. Mechatronics*, vol. 10, no. 6, pp. 648–657, 2005.

[8] G. Coppola and K. Liu, "Control of a unique active vibration isolator with a phase compensation technique and automatic on/off switching," *J. Sound Vibr.*, vol. 329, pp. 5233–5248, 2010.

[9] I. M. Díaz and P. Reynolds, "On-off nonlinear active control of floor vibrations," *Mechan. Syst. Signal Process.*, vol. 24, pp. 1711–1726, 2010.

[10] C. Ding, A. A. H. Damen, and P. P. J. Van den Bosch, "Robust vibration isolation by frequency-shaped sliding surface control with geophone dynamics," in *Proc. Conf. IEEE Ind. Electron. Soc.*, 2010, pp. 211–216.

[11] M. F. Heertjes, F. L. M. Cremers, M. Rieck, and M. Steinbuch, "Nonlinear control of optical storage drives with improved shock performance," *Control Eng. Pract.*, vol. 13, pp. 1295–1305, 2005.

[12] M. F. Heertjes, K. De Graaf, and J.-G. Van der Toorn, "Active vibration isolation of metrology frames; A modal decoupled control design," *J. Vibr. Acoust.*, vol. 127, pp. 223–233, 2005.

[13] D. Hrovat, "Survey of advanced suspension developments and related optimal control applications," *Automatica*, vol. 33, no. 10, pp. 1781–1817, 1997.

[14] F. Kerber, S. Hurlebaus, B. M. Beadle, and U. Stöbener, "Control concepts for an active vibration isolation system," *Mechan. Syst. Signal Process.*, vol. 21, pp. 3042–3059, 2007.

[15] D. Karnopp, "Active and semi-active vibration isolation," *J. Mechan. Design*, vol. 177, pp. 177–185, 1995.

[16] H. K. Khalil, *Nonlinear Systems*, 3rd ed. Upper Saddle River, New York: Prentice-Hall, 2002.

[17] S. M. Lee and J. H. Park, "Robust stabilization of discrete-time nonlinear Lure'e systems with sector and slope restricted nonlinearities," *Appl. Math. Comput.*, vol. 200, pp. 429–436, 2008.

[18] D. Materassi, G. Innocenti, R. Genesio, and M. Basso, "A composite circle criterion," in *Proc. 46th Conf. Decision Control*, 2007, pp. 4459–4464.

[19] A. Preumont, *Vibration Control of Active Structures – An Introduction*, 2nd ed. Norwell, MA: Kluwer, 2004.

[20] A. Shamsi and N. Choupani, "Continuous and discontinuous shock absorber control through skyhook strategy in semi-active suspension system (4dof model)," *Eng. Technol.*, vol. 41, pp. 745–749, 2008.

[21] E. D. Sontag, "On the input-to-state stability property," *Euro. J. Control*, vol. 1, pp. 24–36, 1995.

[22] A. Wills, D. Bates, A. Fleming, B. Ninness, and S. O. R. Moheimani, "Model predictive control applied to constraint handling in active noise and vibration control," *IEEE Trans. Control Syst. Technol.*, vol. 16, no. 1, pp. 3–12, Jan. 2008.
[23] V. A. Yakubovich, G. A. Leonov, and A. K. h. Gelig, *Stability of Stationary Sets in Control Systems with Discontinuous Nonlinearities*. Singapore: World Scientific, 2004.
[24] M. Yasuda, T. Osaka, and M. Ikeda, "Feedforward control of a vibration isolation system for disturbance suppression," presented at the Conf. Decision Control, Kobe, Japan, 1996.
[25] Y. Zhang, A. G. Alleyne, and D. Zheng, "A hybrid control strategy for active vibration isolation with electrohydraulic actuators," *Control Eng. Pract.*, vol. 13, pp. 279–289, 2005.
[26] L. Zuo, J.-J. E. Slotine, and S. A. Nayfeh, "Experimental study of a novel adaptive controller for active vibration isolation," in *Proc. Amer. Control Conf.*, 2004, pp. 3863–3868.

Marcel F. Heertjes received the M.Sc. and Ph.D. degrees in mechanical engineering from the Department of Mechanical Engineering, Eindhoven University of Technology, Eindhoven, The Netherlands, in 1995 and 1999, respectively.

In 2000, he joined the Philips Centre for Industrial Technology, Eindhoven. In 2007, he joined ASML, Mechatronics Development, in Veldhoven and (part-time) the Control System Technology and the Dynamics and Control Groups with the Department of Mechanical Engineering, Eindhoven University of Technology. As first author, he has published around 50 refereed papers and holds around 20 patents. He is one of the originators of the concepts of variable gain control. His current research interests include the control of industrial motion systems with special attention for nonlinear control, feedforward/learning control, and machine-in-the-loop controller optimization and self-tuning.

Ismail Hakki Sahin received the B.S. and M.S. degrees in mechanical engineering from Bogaziçi University, Istanbul, Turkey, in 2008 and 2010, respectively.

In 2010, he joined the Hybrid and Networked Systems Group, Mechanical Engineering Department, Eindhoven University of Technology, Eindhoven, The Netherlands. In 2011, he joined the military service in the Turkish Naval Forces as an engineer second Lieutenant.

Nathan van de Wouw was born in 1970, in Eindhoven, The Netherlands. He received the M.Sc. degree (with honors) and Ph.D. degree in mechanical engineering from the Eindhoven University of Technology, Eindhoven, the Netherlands, in 1994 and 1999, respectively.

From 1999 to 2011, he has been affiliated with the Department of Mechanical Engineering, Eindhoven University of Technology in the group of Dynamics and Control as an Assistant/Associate Professor. In 2000, he was with Philips Applied Technologies, Eindhoven, The Netherlands, and, in 2001, he was with the Netherlands Organization for Applied Scientific Research (TNO), Delft, The Netherlands. He has held positions as a visiting Professor with the University of California, Santa Barbara, in 2006 and 2007, at the University of Melbourne, Australia, in 2009 and 2010, and at the University of Minnesota, in 2012. He has published a large number of journal and conference papers and the books *Uniform Output Regulation of Nonlinear Systems: A convergent Dynamics Approach* with A.V. Pavlov and H. Nijmeijer (Birkhauser, 2005) and *Stability and Convergence of Mechanical Systems with Unilateral Constraints* with R.I. Leine (Springer-Verlag, 2008). His current research interests include the analysis and control of nonlinear/non-smooth systems and networked control systems.

W. P. Maurice H. Heemels received the M.Sc. degree in mathematics and the Ph.D. degree (both with the highest distinction) from the Eindhoven University of Technology (TU/e), Eindhoven, the Netherlands, in 1995 and 1999, respectively.

From 2000 to 2004, he was with the Electrical Engineering Department, TU/e, as an Assistant Professor, and from 2004 to 2006 with the Embedded Systems Institute (ESI) as a Research Fellow. Since 2006, he has been with the Department of Mechanical Engineering, TU/e, where he is currently a Full Professor and the chair of the Hybrid and Networked Systems Group. He held visiting research positions at the Swiss Federal Institute of Technology (ETH), Zurich, Switzerland (2001) and at the University of California at Santa Barbara (2008). In 2004, he was also at the Research and Development Laboratory, Océ, Venlo, The Netherlands. His current research interests include hybrid dynamical systems, networked control systems, event-triggered control and constrained systems including model predictive control.

Dr. Heemels is an Associate Editor for the journals *Automatica* and *Nonlinear Analysis: Hybrid Systems* and serves as the General Chair of the 4th IFAC Conference on Analysis and Design of Hybrid Systems 2012 in Eindhoven, The Netherlands.